Nuclear Instruments and Methods 193 (1982) 549–556
North-Holland Publishing Company

GAMMA-CALIBRATION OF NE 213 SCINTILLATION COUNTERS

G. DIETZE and H. KLEIN
Physikalisch-Technische Bundesanstalt, D-3300 Braunschweig, Fed. Rep. Germany

Received 6 July 1981

A method is described of calibrating the light output of NE 213 scintillation detectors by means of "monoenergetic" photon sources. The position of the Compton edge can be precisely determined by comparing the measured pulse-height spectrum with a Monte Carlo simulated distribution properly folded with the pulse-height dependent resolution. For the various sizes of scintillator systems the position of the Compton edge relative to the position of the maximum and the half maximum of the distribution is tabulated in dependence on relevant detector resolutions. The results may be used to determine the resolution function and to check the linearity of the light output.

1. Introduction

The NE 213 * liquid scintillator is often used for neutron monitoring, time-of-flight measurements and neutron spectroscopy including spectrum unfolding techniques, mainly because of its high detection efficiency and excellent n–γ discrimination properties. Complex neutron energy spectra can be extracted by unfolding the pulse height spectra on the basis of reference spectra measured with monoenergetic neutrons [1].

If alternatively the response matrix is calculated by means of Monte Carlo methods the strongly nonlinear dependence of the light output on the energy of the secondary charged particles has to be considered.

These light output functions have been extensively studied [2–6] and are usually related to the light output function for electrons, which is almost linear for electron energies $E_e \geqslant 40$ keV and may be approximated by $L = c(E_e - E_0)$. The small offset energy $E_0 = 5$ keV [7] takes into account the nonlinearity due to quenching effects in NE 213 for small electron energies. The scaling parameter c (in MeV^{-1}) may be chosen arbitrarily. In this paper the pulse height of the scintillation system is calculated and measured in relation to the effective electron energy $(E_e - E_0)$ ($c = 1$ MeV^{-1}).

Verbinski et al. [3] and other authors [5,19] have defined one light unit from the Compton spectrum of the 1.275 MeV photons of a ^{22}Na-source corresponding to a scaling parameter $c = 0.80$ MeV^{-1}. Their results, however, cannot be compared without renormalizing the light output function, because different concepts were used to determine the position of the Compton edge (see section 4).

In this paper the influence of the pulse height resolution on the position of the Compton edge is discussed for various detector sizes and photon energies. Means of analysing Compton spectra with respect to the energy scale and the resolution are given.

* Nuclear Enterprise Ltd., Edinburgh, Scotland.

2. Monte Carlo calculation

2.1. Compton distribution

For photon energies up to 3 MeV Compton scattering is the dominating process in a NE 213 scintillator which is a toluene-based solution. For monoenergetic photons of energy E_γ Compton electrons are produced up to an energy $E_e \leqslant 2E_\gamma^2/(0.511 + 2E_\gamma)$, all energies given in MeV. The sharp upper edge of the well known Compton distribution is used for energy calibration. But due to multiple scattering effects the theoretical shape must be modified and finally folded with the pulse height resolution.

Both effects strongly depend on the size of the detector system and the photon energy. The final

0029-554X/82/0000–0000/$02.75

shape of the electron energy distribution is therefore separately calculated by means of a Monte Carlo simulation for any particular geometrical set-up and the diverse photon sources generally used for calibration.

2.2. Geometrical set-up

NE 213 liquid scintillators with Al-capsules are under investigation (BA1-type of Nuclear Enterprises). A simplified model of the detector system is constructed for the Monte Carlo calculation of the photon response function (fig. 1). The cylindrical Al-vessel contains the same scattering material as the real capsule and has to be included because of inscattering effects.

The scintillators are connected to photomultipliers via lucite light pipes. Partial coating of the light guide reduces remarkably the dependence of the light transmission on the locus of the light production [8]. In this case the light transport does not have to be included in the Monte Carlo simulation.

If conical light pipes are used to match the radii of the scintillator and the photocathode, cylindrical light guides of the same mass are simulated for simplicity. Separate calculations have shown that the shape of the light guide does not influence the pulse height distribution, especially near the Compton edge.

The parameters of all scintillator systems investigated in this work are listed in table 1.

2.3. Monte Carlo calculation

The pulse height spectra are calculated using our three-dimensional photon transport code GRESP. By means of Monte Carlo methods, the course of photons emitted by a source anywhere outside the detector system is followed within the scintillator system including the Al-vessel and the light pipe, until the photons escape or the energy of scattered photons reaches the cut-off energy of 2 keV. The interactions are randomly chosen taking into account Compton scattering and photoelectric absorption. Pair production at hydrogen and carbon atoms can be neglected for photon energies $E \leqslant 3$ MeV [9].

Some approximations are introduced into these calculations concerning the secondary electrons. It is assumed that the electrons deposit all their energy inside the scintillator volume as long as the distance of the interaction to the boundary is greater than the mean range [9]. Energy losses due to bremsstrahlung are neglected. Wall effects are included twice. Electrons produced in the scintillator may pass the Al-wall. Alternatively electrons may be produced in the Al-vessel and stopped in the scintillator. In both cases only the energy loss within the scintillator is taken into account. GRESP finally calculates the distribution of the integrated light output on the basis of a linear relation to the electron energy as mentioned above.

As an example, fig. 2 shows the pulse height spectrum for 0.662 MeV photons of a ^{137}Cs source to be expected in the detector of greatest volume (detector 4 in table 1). Multiple photon scattering strongly

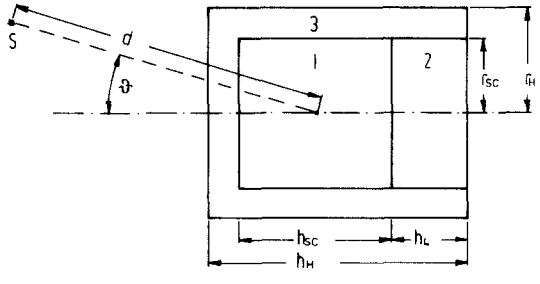

Fig. 1. Outline of the detector geometry used for Monte Carlo calculations: (1) NE 213; (2) lucite; (3) aluminum; (S) photon source.

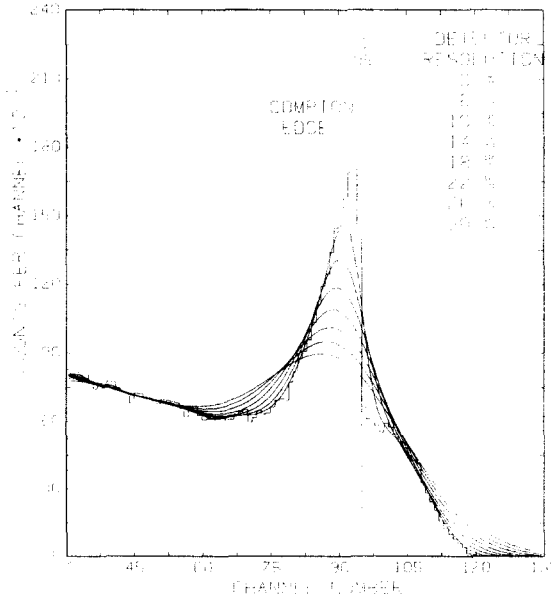

Fig. 2. Calculated Compton electron spectrum from a ^{137}Cs photon source in a large NE 213 detector (detector 4 of table 1) folded with various resolutions.

Table 1
Detector data used for the Monte Carlo calculations: NE 213 scintillator [a], ρ = 0.874 g/cm^3; mole fraction, H 54.8%, C 45.2%. lucite light pipe, ρ = 1.18 g/cm^3; mole fraction, H 52.5%, C 47.5%. The scintillators are in BA1 type Al housings.

No.	Scintillator		Al-housing		Light pipe		Detector resolution			Multiplier type [b]
	radius (cm)	height (cm)	outer radius (cm)	height (cm)	radius (cm)	height (cm)	α (%)	β (%)	γ (%)	
1	1.90	3.80	2.41	5.97	1.90	2.00	1.5	9.0	0.2	XP 2020
2	2.53	5.07	2.91	8.04	2.53	2.80	1.2	10.0	0.2	XP 2020
3	6.35	5.07	6.81	8.47	6.35	3.00	–	–	–	–
4	12.70	5.08	13.70	10.88	12.70	5.20	5.6	18.0	0.2	XP 2041

a) Nuclear Enterprise Ltd., Edinburgh, Scotland.
b) Valvo GmbH, Hamburg, FRG.

enhances the Compton edge and fills the spectrum above this peak.

2.4. Pulse height resolution

The calculated pulse height spectra must be folded with the pulse height dependent resolution of the detector system under investigation. The resolution ΔL (fwhm) of the integrated detector signal L is given by [7,8,10]

$$\Delta L/L = (\alpha^2 + \beta^2/L + \gamma^2/L^2)^{1/2}$$

including independent contributions due to

(a) the locus dependent light transmission (α) from the scintillator to the photocathode;

(b) the statistical behaviour of the light production, attenuation, photon–electron conversion and electron amplification (β); and

(c) all noise contributions due to the photo-multiplier (dark current) and electronic amplifiers (γ).

The resolution parameters depend on the properties of the detector components (e.g. scintillator and light guide material, phototube) as well as on constructive details (e.g. shape and coating of the light guide, base of the phototube). Thus the parameters for any particular detector set-up must be determined either experimentally by means of monoenergetic photon and neutron sources or theoretical estimates [8].

2.5. Position of the Compton edge

The strong influence of the resolution on the position of the Compton edge with respect to the position of the maximum (L_{max}) or the half height of this maximum ($L_{1/2}$) at the upper part of the Compton distribution is also demonstrated in fig. 2. This effect is systematically studied for various detector sizes (table 1) and photon sources (table 2). As essential results of the Monte Carlo calculation the relative position of the maximum and the half-maximum with respect to the Compton edge L_c are tabulated for the relevant photon sources with energies between 279 keV and 1.836 MeV (table 3) in dependence on the resolution $\Delta L/L_c$ of the detector system at this energy. As an example, the tendencies are shown for 1.275 MeV photons of ^{22}Na often used for a calibration (fig. 3). The influence of the size of the scintillator is particularly remarkable. The effect of multiple photon scattering within the detector depends on the detector size. The position of the Compton edge is therefore nearer to the half maximum position for small detectors than for large detectors.

Table 2
Data of photon sources used for calibration

Source	E_γ (MeV)	$E_{Compton}$ (MeV)	Halflife $T^{1/2}$
^{203}Hg	0.279	0.146	46.6 d
^{22}Na	0.511	0.341	950.4 d
^{137}Cs	0.662	0.477	30 a
^{54}Mn	0.835	0.639	312.5 d
^{88}Y	0.898	0.699	106.6 d
^{65}Zn	1.115	0.907	244 d
^{22}Na	1.275	1.061	950.4 d
^{24}Na	1.369	1.154	15.0 h
^{40}K	1.461	1.244	1.26 × 10^9 a
^{88}Y	1.836	1.612	106.6 d
^{208}Tl	2.614	2.381	Th-series
^{24}Na	2.754	2.520	15.0 h

Table 3
L_{max}/L_c and $L_{1/2}/L_c$ versus detector resolution ($\Delta L/L$) at the Compton edge for photons from ^{88}Y, ^{22}Na, ^{137}Cs and ^{203}Hg

	$\Delta L/L$ (%)	Detector 1		Detector 2		Detector 3		Detector 4	
		L_{max}/L_c	$L_{1/2}/L_c$	L_m/L_c	$L_{1/2}/L_c$	L_m/L_c	$L_{1/2}/L_c$	L_m/L_c	$L_{1/2}/L_c$
$^{88}Y_{1.8}$	2	0.984	1.004	0.984	1.004	0.985	1.008	0.985	1.011
	6	0.963	1.014	0.964	1.016	0.971	1.026	0.975	1.034
	10	0.945	1.022	0.948	1.026	0.960	1.038	0.968	1.047
	14	0.927	1.030	0.932	1.035	0.948	1.048	0.960	1.059
	18	0.907	1.038	0.915	1.043	0.926	1.058	0.949	1.070
	22	0.885	1.046	0.898	1.051	0.917	1.067	0.935	1.080
$^{88}Y_{0.89}$	6	0.960	1.014	0.959	1.014	0.966	1.027	0.969	1.037
	10	0.941	1.024	0.941	1.027	0.953	1.045	0.960	1.059
	14	0.923	1,033	0.923	1.037	0.942	1.058	0.952	1.074
	18	0.906	1.043	0.906	1.046	0.931	1.070	0.945	1.087
	22	0.888	1.050	0.889	1.055	0.917	1.081	0.936	1.098
	26	0.868	1.058	0.869	1.062	0.903	1.091	0.924	1.109
	30	0.847	1.066	0.848	1.070	0.886	1.100	0.911	1.120
^{237}Cs	10	0.939	1.025	0.939	1.026	0.950	1.046	0.955	1.059
	14	0.922	1.035	0.922	1.038	0.949	1.063	0.948	1.079
	18	0.905	1.045	0.905	1.049	0.927	1.076	0.941	1.095
	22	0.886	1.053	0.887	1.059	0.913	1.088	0.933	1.108
	26	0.867	1.061	0.869	1.067	0.901	1.098	0.924	1.120
	30	0.846	1.069	0.849	1.074	0.886	1.108	0.912	1.130
	34	0.824	1.076	0.828	1.081	0.869	1.117	0.899	1.141
$^{22}Na_{0.51}$	14	0.918	1.033	0.917	1.036	0.933	1.061	0.938	1.076
	18	0.900	1.043	0.900	1.047	0.921	1.077	0.931	1.096
	22	0.881	1.052	0.882	1.058	0.909	1.090	0.924	1.110
	26	0.860	1.060	0.862	1.066	0.895	1.101	0.914	1.124
	30	0.840	1.067	0.842	1.074	0.883	1.112	0.903	1.136
	34	0.817	1.074	0.818	1.082	0.869	1.121	0.892	1.147
^{203}Hg	15	0.905	1.033	0.903	1.037	0.917	1.060	0.925	1.077
	20	0.879	1.044	0.884	1.051	0.900	1.081	0.910	1.104
	25	0.852	1.055	0.859	1.064	0.883	1.100	0.899	1.125
	30	0.824	1.064	0.832	1.077	0.866	1.115	0.886	1.145
	35	0.791	1.073	0.802	1.087	0.848	1.129	0.873	1.162
	40	0.763	1.080	0.775	1.094	0.829	1.141	0.859	1.176

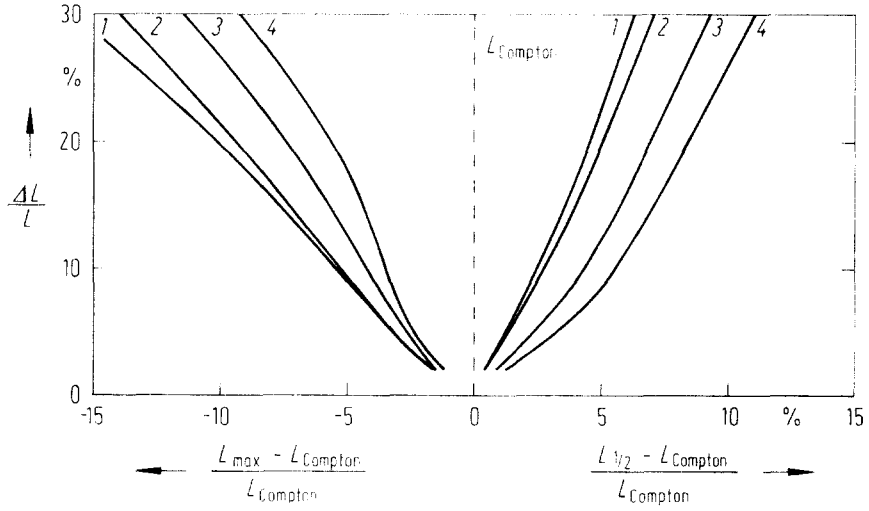

Fig. 3. The position of the maximum L_{max} and of the half maximum $L_{1/2}$ relative to the Compton edge $L_{Compton}$ versus the detector resolution $\Delta L/L$ for detectors of various size (detectors 1–4 of table 1) and photons from ^{22}Na, $E_\gamma = 1.275$ MeV.

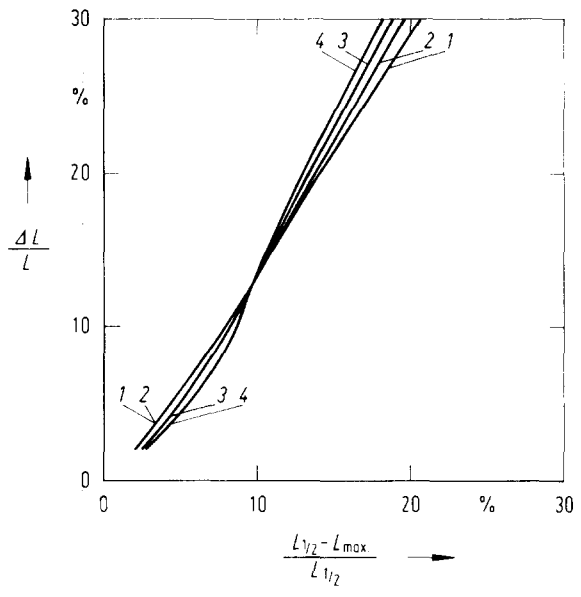

Fig. 4. Pulse height resolution for detectors of various size (detectors 1–4 of table 1) as a function of $(L_{1/2} - L_{max})/L_{1/2}$ derived from Compton electron spectra calculated for E_γ = 1.275 MeV.

Similar graphs can be obtained for all photon energies listed in table 3. For intermediate detector geometries the theoretical data may be interpolated. In any case the best analysis is obtained by comparing the experimental pulse height spectra with properly folded Monte Carlo distributions.

Alternatively the theoretical results shown in table 3 may be used to extract the pulse height resolution from experimental Compton spectra. As again demonstrated for ^{22}Na in fig. 4, the resolution can be simply determined by the relative difference $(L_{1/2} - L_{max})/L_{1/2}$ almost independent of the size of the scintillator. As a rough estimate

$$\Delta L/L \text{ (fwhm)} \simeq 1.5(L_{1/2} - L_{max})/L_{1/2}$$

may be used, independent of the photon energy and the detector size.

3. Experimental data

NE 213 liquid scintillators of different size have been studied (detectors 1, 2 and 4 of table 1). In general ^{22}Na, ^{88}Y and ^{137}Cs photon sources were used. In the case of the large volume system (detector 4), the most intensive background radiation from ^{40}K and ^{208}Tl could also be analysed, whereas short-lived sources such as ^{65}Zn, ^{54}Mn and ^{24}Na and ^{203}Hg, in particular, were not available for all investigations.

3.1. Resolution function $\Delta L/L$

The resolution function $\Delta L/L$ was determined from experimental Compton spectra using the methods given in sections 2.4 and 2.5. As shown in fig. 5 for the small volume (detector 2) and the large volume (detector 4) detectors the photon data agree very well with the resolution data extracted from proton recoil spectra produced by monoenergetic neutrons. In addition the resolution function of the smallest scintillator (detector 1) is shown for comparison. The resolution parameters α, β, γ are listed in table 1.

The values of α for the various detectors are almost the same as those from light transport calculations [8] which were carried out to optimize the setup. The influence of the dark current and electronic noise parameter (γ) can be separately determined from the width of a pulse generator line fed into the preamplifier as the first electronic module behind the phototube. This contribution can usually be neglected in the energy range generally covered.

The dominating contribution (β) is influenced by various statistical processes in scintillation detectors [10] which have to be considered as a cascade:

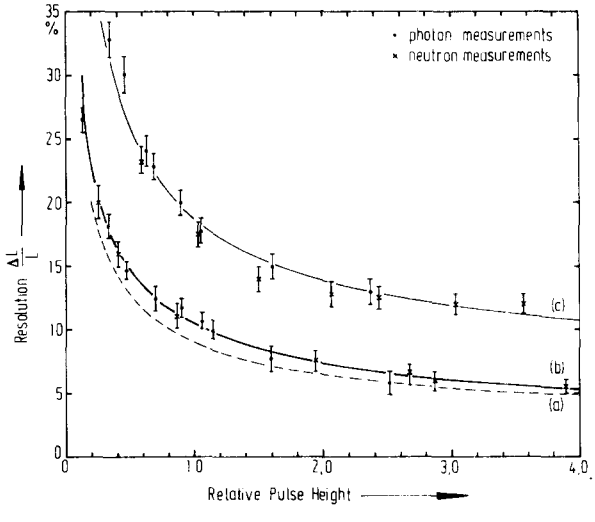

Fig. 5. Pulse height dependent resolution $\Delta L/L$ for the NE 213 scintillation detectors 1 (a), 2 (b) and 4 (c) of table 1: photon measurements depicted by full points and neutron measurements by crosses.

(a) the number of photons $N_{ph}(E)$ produced by a secondary charged particle such as a Compton electron or a recoil proton (Poisson distribution);

(b) the mean probability $\bar{\eta}_t \leqslant 1$ for the transmission of the photon to the photocathode. Only for setups with partially coated light guides is a symmetric pulse height distribution obtained [8];

(c) the partial conversion into photoelectrons with the mean quantum efficiency $\bar{\eta}_q \leqslant 0.3$;

(d) the collection of the photoelectrons to the first dynode with an efficiency $\bar{\eta}_c \leqslant 1.0$; and

(e) the electron multiplication in the dynode chain with a mean gain factor $\bar{G} \gg 1$.

Assuming an ideal statistical behaviour of all the cascade processes (a)–(d), the number of collected photoelectrons

$$N_{ce} = N_{ph}\bar{\eta}_t\bar{\eta}_q\bar{\eta}_c$$

will be Poisson distributed with a relative variance $v_{ce} = 1/N_{ce}$.

As the phototubes are generally used with a high gain $g_1 \gg 1$ at the first dynode and a mean gain g of the following $(n-1)$ stages with $g_1 > g > 1$, the total gain $\bar{G} \approx g_1 g^{(n-1)}$ has a relative variance [10–12]

$$v_g \approx \frac{g}{g_1(g-1)} .$$

The statistical contribution may therefore be estimated to be:

$$\beta/L^{1/2}(\text{fwhm}) \approx 2.35 \left[\left(1 + \frac{g}{g_1(g-1)}\right) / N_{ce}\right]^{1/2} .$$

Similar phototubes with respect to the quantum efficiency and the dynode chain have been used for the various detectors. Assuming the photon production $N_{ph}(E)$ to be independent of the size of the scintillator, the product of the light transmission and the electron collection must cause the increase of the parameter β by a factor of about 2 as determined for the large volume detector 4 with respect to the small systems (detectors 1 and 2). Whereas a reduction of the light transmission $\bar{\eta}_t$ by a factor of about 2.5 is expected from light transport calculations [8] the collection efficiency of the large plane phototube XP2041 seems to be reduced to about 55–60% * with respect to the small type XP2020 ($\bar{\eta}_c \sim 0.9$).

* Not specified by the manufacturer Valvo, Hamburg, FRG.

3.2. Compton edge position

The position of the Compton edge can best be determined if the properly folded theoretical distribution is fitted to the experimental pulse height spectrum by a least square fit including only the region of the Compton edge. Defining the pulse height for electrons of energy $(E_e - E_0) = 1$ MeV with the offset energy $E_0 = 5$ keV [7] as one light unit, we find the expected linear relation within uncertainties of ±1% (fig. 6, curves a and c) for the small and the large volume detectors. But for one detector (detector 2) a nonlinearity up to 12% was obsered for energies $E_e \leqslant 500$ keV (fig. 6, curve b). As this nonlinearity remained at the same total charge at the anode

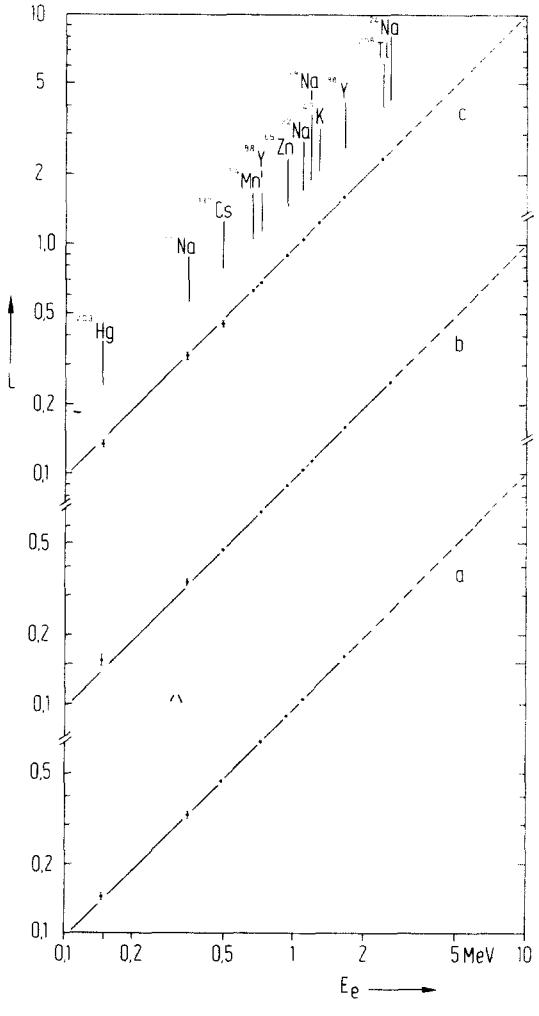

Fig. 6. Pulse height to electron energy relationship for detector 1 (a), 2 (b) and 4 (c) of table 1. The photon sources are indicated. The uncertainty is mostly <1%.

of the photomultiplier if a lower gain was used, the effect seems to indicate a charge-dependent gain or decoupling at the 10th (of 14) dynode. Further investigations are needed including Compton coincidence measurements or measurements by means of extremely linear light pulsing systems to cover the full dynamic range of E_e = 50 keV up to E_e = 5 MeV.

3.3. Compton spectra

The experimental conditions for the measurements must be chosen carefully. Photon sources with low mass backings should be taken to avoid photons of degraded energy [14,15]. Background radiation must be subtracted. Photon backscattering from the surroundings has to be considered, particularly for measurements in small rooms. In this case background measurements with a shadow shield between the photon source and the detector are necessary. The Monte Carlo calculations reproduce almost the measured pulse-height spectra even for complex photon sources.

For the smallest detector, fig. 7 shows very good agreement between experimental data and a Monte Carlo simulation folded with a resolution function according to table 1, for two photon energies of the ^{88}Y source (see table 2). Both Compton spectra are calculated independently. Besides the position and the shape of the Compton edge the branching ratio [15] is reproduced within a 5% uncertainty. The deviation for small energies $E_e \leqslant 100$ keV may be due to the geometrical set-up (concrete, source holder etc.), which was not ideal. Similarly, we find a satisfactory description of the composed spectrum

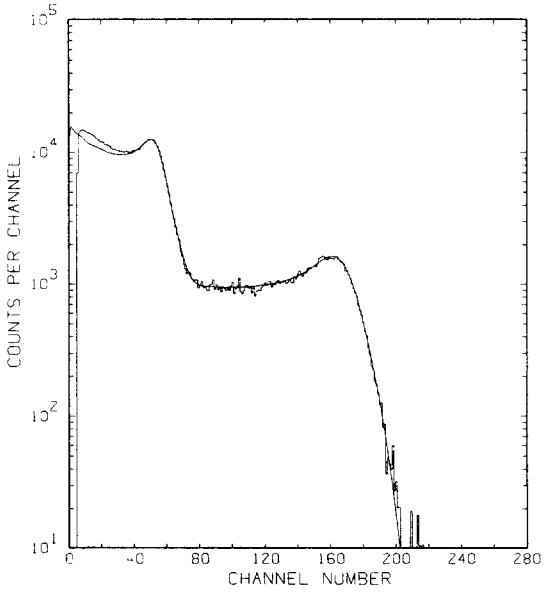

Fig. 8. A measured and a calculated pulse height spectrum for photons from a ^{22}Na source and detector 2.

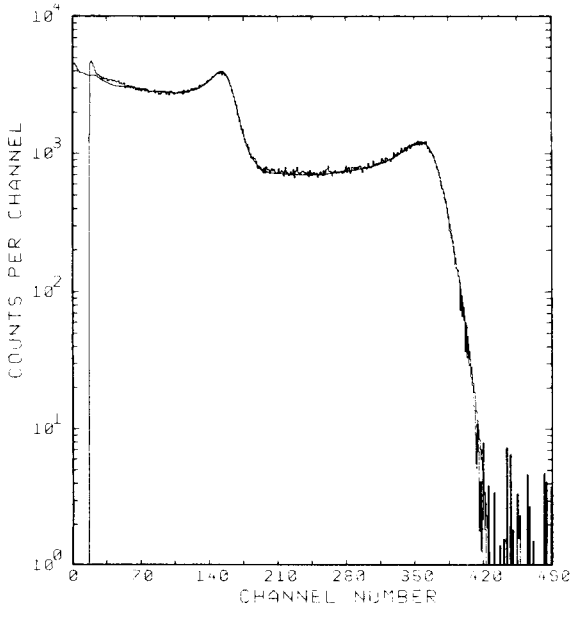

Fig. 7. A measured and a calculated pulse height spectrum for photons from a ^{88}Y source and detector 1.

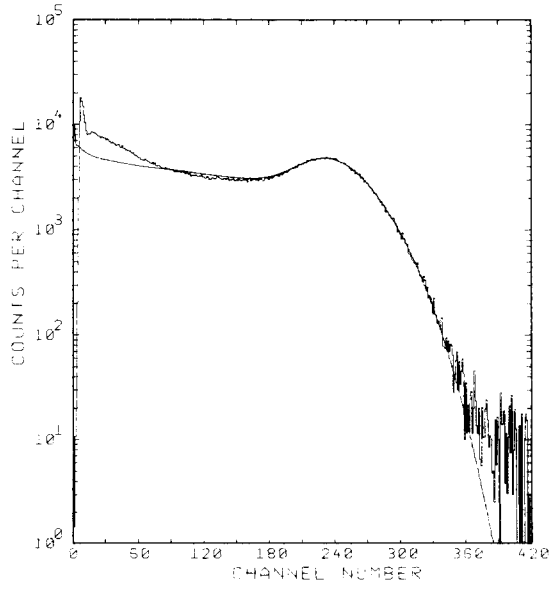

Fig. 9. A measured and calculated pulse height spectrum for photons from a ^{137}Cs source and detector 4.

of a ^{22}Na-source for the detector 2 (fig. 8). The relative intensity of the annihilation quanta, which cannot generally be specified [15], may be extracted for this special arrangement.

Finally in fig. 9, the pulse height spectrum of the monoenergetic source ^{137}Cs is compared with calculations for the large volume detector 4. The photon source has been positioned on the scintillator axis at a distance of 1 m. The background has been measured and subtracted using a shadow shield.

4. Conclusion

Monte Carlo calculations of photon response spectra are described. The strong influence of the scintillator size is discussed for photon energies up to 2.75 MeV. Table 3 includes all relevant information for extracting the pulse height dependent resolution $\Delta L/L$ from experimental pulse height spectra. Assuming satisfactory counting statistics, the maximum Compton electron energy for photon scattering can be identified with an uncertainty $\delta L_c/L_c < 1\%$.

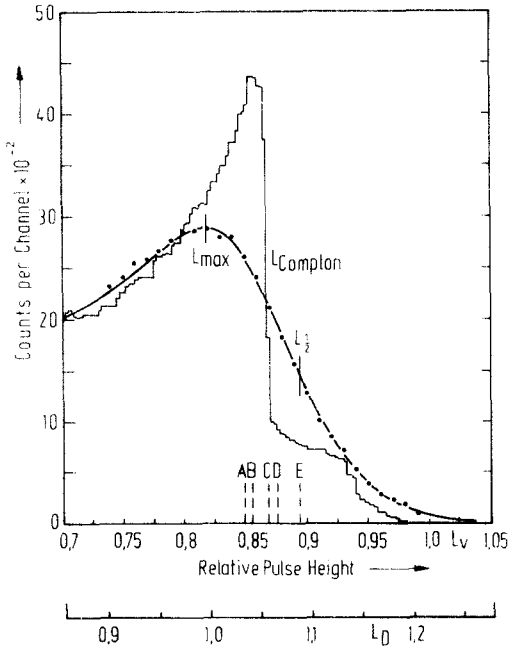

Fig. 10. A pulse height spectrum for photons from ^{22}Na, E_γ = 1.275 MeV, calculated for a NE 213 detector, 4.6 cm in height and 4.6 cm in diameter (histogram). The properly folded spectrum (full line) fits Verbinski's data points [3]. The broken lines give the Compton edge positions as used by different authors. A, refs. 3, 17; B, ref. 16; C, this work; D, ref. 18; E, ref. 19, 20. L_V light unit scale used by Verbinski [3], L_D light unit scale used in this work.

In fig. 10, Verbinski's [3] spectrum around the Compton edge from 1.275 MeV photons of ^{22}Na is shown together with a calculated, folded and fitted spectrum. Various authors [3,16–20] have used this photon source for calibration purposes. The differences in their locating of the position of the Compton edge (broken lines) results in differences of the energy scaling of about 5%. Using our calibration method, Verbinski's scaling parameter must also be changed from 0.80 to 0.82 MeV^{-1}.

Applying the results given in section 2.5 the thresholds for neutron measurements can be reproducibly set at selected light output values by means of photon spectroscopy. Similarly, neutron response functions theoretically or experimentally determined may be used with a light output function $L(E_p)$ which can be normalized to the electron light output with an accuracy better than 1%, using various photon sources.

References

[1] Proc. Seminar-Workshop, ORNL/RSIC-40 (1976).
[2] R. Batchelor, W.B. Gilboy, J.B. Parker and H.J. Towle, Nucl. Instr. and Meth. 13 (1961) 70.
[3] V.V. Verbinski, W.R. Burrus, T.A. Love, W. Zobel and N.W. Hill, Nucl. Instr. and Meth. 65 (1968) 8.
[4] K.H. Maier and I. Nitschke, Nucl. Instr. and Meth. 59 (1968) 227.
[5] D.L. Smith, R.G. Polk and T.G. Miller, Nucl. Instr. and Meth. 64 (1968) 157.
[6] K.F. Flynn, L.E. Glendenin, E.P. Steinberg and P.M. Wright, Nucl. Instr. and Meth. 27 (1964) 13.
[7] G. Dietze, IEEE Trans. Nucl. Sci. NS-26 (1979) 398.
[8] H. Schölermann and H. Klein, Nucl. Instr. and Meth. 169 (1980) 25.
[9] P. Marmier and E. Sheldon, Physics of nuclei and particles, vol. I (Academic Press, New York, 1969) p. 179.
[10] P. Sparrmann, J. Lindskog and A. Marelius, Nucl. Instr. and Meth. 41 (1966) 299.
[11] E. Breitenberger, Prog. Nucl. Phys. 4 (1955) 56.
[12] M.D. Hull, Photomultipliers, Application Book (N.V. Philips Gloeilampenfabrieken, Hamburg, 1970).
[13] F.J. Lynch, IEEE Trans. Nucl. Sci. NS-22 (1975) 58.
[14] N.A. Lurie, L. Harris, Jr., and I.C. Young, Nucl. Instr. and Meth. 129 (1975) 543.
[15] K. Debertin, U. Schötzig, K.-F. Walz and H.M. Weiss, PTB-Mitteilungen 87 (1977) 22.
[16] H.H. Knox and F.G. Miller, Nucl. Instr. and Meth. 101 (1972) 519.
[17] R.H. Johnson, D.T. Ingersoll, B.W. Wehring and J.J. Dorning, Nucl. Instr. and Meth. 145 (1977) 337.
[18] L.E. Beghian, S. Wilensky and W.R. Burrus, Nucl. Instr. and Meth. 35 (1965) 34.
[19] J.L. Fowler, J.A. Cookson, M. Hussain, R.B. Schwartz, M.T. Swinhoe, C. Wise and C.A. Uttley, Nucl. Instr. and Meth. 175 (1980) 449.
[20] J.B. Czirr, D.R. Nygren and C.D. Zafiratos, Nucl. Instr. and Meth. 31 (1964) 226.